Polymer Bulletin (2024) 81:17213–17232
https://doi.org/10.1007/s00289-024-05498-1

ORIGINAL PAPER

How does heat generation affect the cut and chip wear of rubber?

Nikolas Ryzí[1] · Radek Stoček[1] · Jaroslav Maloch[1] · Martin Stěnička[1]

Received: 11 July 2024 / Revised: 22 August 2024 / Accepted: 15 September 2024 /
Published online: 25 September 2024

Abstract

Tire wear is a fracture process that has a decisive impact on tire life and on the environment. When a tire rolls, a heating process occurs due to friction caused by the viscoelastic rubber sliding over uneven road. This process occurs globally in the contact patch area and locally around the asperity tips, heating the tread and transferring heat to the surrounding material. On roads with a good quality pavement, the stress, and therefore the heat, is evenly distributed throughout the rubber material of the tire, which has a direct effect on fatigue wear. In contrast, unevenly distributed stress, and therefore heat, is generated in the tread when the tire rolls and slides over sharp asperities in rough terrain. This leads to very pronounced, unstable fracture processes that cause unevenly distributed wear, known as cut and chip (CC). The extent of heat generation or temperature evolution and its effect on CC wear have not yet been investigated and described in scientific publications. Therefore, this study firstly presents the detailed characterization of the influence of temperature development on the CC wear of a styrene–butadiene rubber, which commonly is used in treads of consumer tires. The investigations were carried out using the unique instrumented cut and chip technique in combination with a high-speed thermography.

Keywords Wear · Rubber · Tire · Cut and chip · Heat · Temperature · Testing

Introduction

Loads and processes in the contact area between a tire contact patch and the road surface determine the real load conditions of a tire. The material of the tire tread is subject to wear and abrasion. In general, a tire undergoes several wear mechanisms during its use, which essentially consist of fatigue wear, abrasion wear and

✉ Nikolas Ryzí
n_ryzi@utb.cz

[1] Centre of Polymer Systems, University Institute, Tomas Bata University in Zlín, tř. Tomáše Bati 5678, Zlín 760 01, Czech Republic

cutting wear [1, 2]. These mechanisms can be distinguished according to their different severities. Fatigue wear occurs on smooth roads under moderate loads, while abrasive or cutting wear becomes significant with increasing road roughness [3–5]. As the tire rolls over the road surface, the viscoelastic properties of the tread rubber lead to energy dissipation, which is generally the cause of tire heating. In addition, acceleration, deceleration, cornering and alignment of the axle geometry generate shear forces that increase the energy dissipation compared to the uniform rolling of the tire. Shear forces are the main cause of tire wear, and it is, therefore, clear that heat development is part of the wear process and directly affects its mechanism. Wear and heating occur simultaneously in the stress concentration area around the tire footprint and locally around the asperity tips. The wear theory can be described by the so-called brush model [6–8], which can be extended to include heat evolution, as shown schematically in Fig. 1.

The complete mechanism can be divided into six phases. In the 1st phase, an area of the tread is illustrated just before the contact with one asperity of the ground. Once in contact, illustrated in the 2nd phase, the inequality pierces the rubber at point A causing local stress concentration in the rubber volume around the asperity

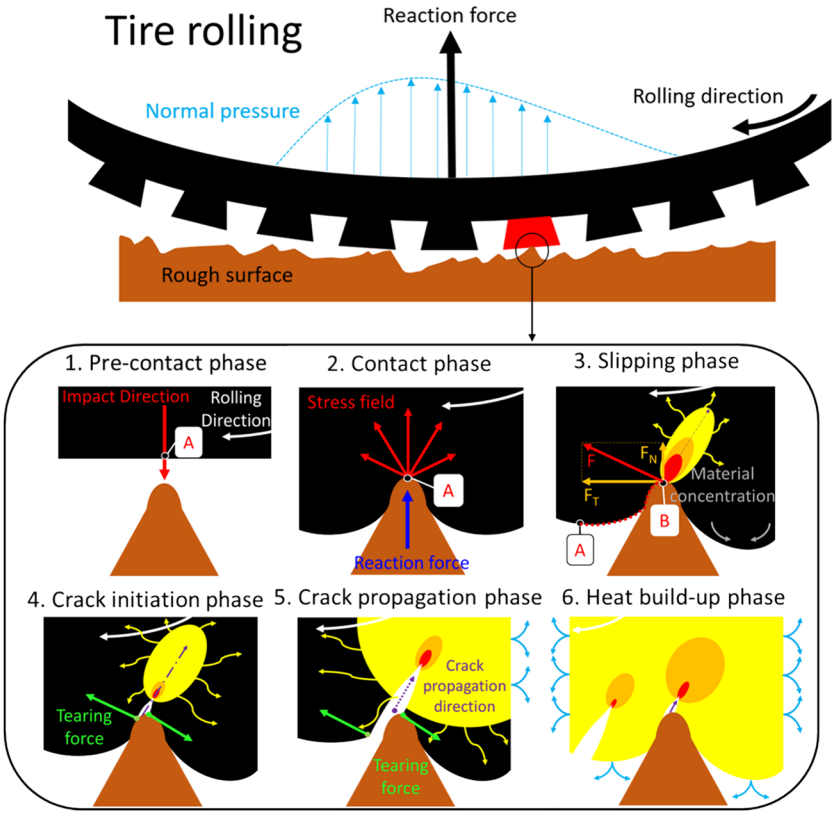

Fig. 1 Illustration of the deformation and self-heating process during tire's impact with sharp asperity

tip. The sharper the asperity, the greater the deformation in the immediate vicinity of the tip and the greater the stress in the surrounding volume. The 3rd phase is the slippage of the tread rubber along the asperity. This slippage is visualized by the red dotted line from point *A* to point *B*. During the slip, friction between the surface of the asperity and the rubber is present and subsequently results in significant shear forces, *F*, in tangential direction to rotation, which causes significant deformations of the rubber and maximum stress concentration perpendicular to this force. Due to the friction and viscoelastic behaviour of the rubber, an enormous amount of energy is dissipated in this vertical direction, which leads to the initiation of a crack and further conversion into heat at the crack tip, as shown in the 4th phase. The 5th phase is characterized by the propagation of the resulting crack and the induction of additional heat for each rolling sequence. Through a combination of rolling and slipping, new cracks are induced parallel to those already formed. This newly initiated crack at its tip acts as another area of local heat concentration; whereas, this process being illustrated in the 6th phase. The formation of numerous cracks then destroys the entire tread, and the propagation of all cracks is significantly accelerated. At the same time, thermal equilibrium is achieved because the heat generated by the mechanical load equals the heat loss to the surroundings.

As a result of the increased heat generation, it is to be expected that the softer the material becomes, the more energy is dissipated and less energy is available to promote crack formation and propagation through the abrasion process itself. From the above, it is clear that as the roughness of the pavement increases, the value of dissipated energy converted into heat also changes, with heat generation increasing as the roughness of the pavement increases. While on ordinary roads with quality pavement, due to the evenly distributed stress in the tread across the contact patch, uniform heat generation is assumed, and thus, its effect on fatigue wear is to be expected, high and unevenly distributed stresses are generated in the tread when the tire rolls and slides over sharp bumps in rough terrain. This leads to very pronounced, unevenly distributed wear, known as cut and chip (CC). It is the high stresses in rough terrain that are the prerequisite for the enormous heating of the tread and its effects on CC wear. It is, therefore, important for the development of new wear-resistant rubber materials to understand the effect of the heating of the rubber by the varying quality of the road surface on the tire wear process. In this study, only the heat development during the CC wear process is investigated.

An example of a tire subject to permanent CC wear is a robust tire of harvesters, tractors or forestry machines. In general, these seasonal machines are primarily used on rough surfaces with high occurrence of obstacles such are stones, boulders, branches, stumps and other sharp asperities which cause high normal and shear forces during the contact with tire, whose mechanism is described in Fig. 1. Figure 2 shows photographs illustrating real examples of visible CC wear on forest harvester tire treads.

The CC wear mechanism consists of two inter-linked processes. First, the tire is subjected to an impact with a sharp object in simultaneous rotation and slipping of tire tread over the asperity, which induces local forces in the tread. This is due to the fact that the surface of the asperities is very small, while at the same time, high forces act on the tire. Thus, the high torque is unable to capture the small surface

Fig. 2 The cut and chip wear phenomena of a forest harvester tire tread

and slippage occurs. If the resulting force exceeds a threshold force, a crack is initiated. This process is referred to as "cutting". The second process takes place when already initiated cracks or their vicinity comes into contact with a new sharp obstacle which acts as a force trigger when the tire rolls and slips. This time, however, the resulting force acts on the already initiated crack, which, therefore, propagates. If the resulting force is sufficiently large and the tire surface is already distorted to some extent, the crack propagates through the local volume of material and a chunk of the rubber is torn away. This process is referred as "chipping".

The most severe case may occur when the impacting force is substantially higher than the threshold force. In this case, both processes act simultaneously as the crack is initiated and immediately propagated further. This spreading can be very unstable and cause numerous pieces of different sizes to detach immediately from the tread.

Previously, the response of rubber to CC mechanism under laboratory conditions was primarily measured by recording the weight loss of the sample throughout the measurement process as described in [9, 10]. However, this approach is no longer perceived as relevant as the material loss rarely corresponds to the results of the real-life tire tests.

Today's standard is the established instrumented laboratory method for describing rubber behaviour [11]. The method is based on the application of Instrumented Cut and Chip Analyser (ICCA, Coesfeld GmbH & Co. KG, Germany), which is able to perform a measurement of CC wear of rubber material responding to conditions which closely correspond to those during a real-life performance.

It was proved that the ICCA [11, 12] and the CC measuring approach is in a very good correlation with the results from the real-life tire testing [13]. Moreover, using this approach, it was possible for the first time to explain the role of strain-induced crystallisation as a significant contributor to high resistance of natural rubber to CC wear [12].

However, it is also important to focus on other processes that accompany and influence the mechanical behaviour of rubber subjected to the CC mechanism. Thermal processes play a special role [14].

During CC wear, the tread surface is subjected to frictional rolling or sliding on the asperity, which, in combination with the viscoelastic properties of the rubber, leads to the conversion of mechanical energy into heat [15, 16]. As the number of loading cycles increases, the temperature both on the surface and inside the rubber material increases due to the low thermal conductivity of the rubber [15, 17]. The evolution of the heat rise is mainly dependent on the loading conditions [18, 19], the geometry of the test specimen [20] and the rubber composition [21].

It has been shown that under constant loading conditions, the temperature reaches a certain maximum value without further increase and any further heat generated is transferred to the surroundings [22–24]. However, if the rubber fails in the equilibrium temperature state, the temperature in this region will increase locally [24]. This points to additional mechanical processes present during total rupture.

A study [25] showed that for a loaded rubber sample, most of the mechanical work applied to the sample dissipates to thermal energy and a small amount of energy is elastically stored as potential energy. Moreover, in the identical paper, it was shown that a small amount of thermal energy is immediately dissipated to the surroundings. This heat loss depends on the total thermal energy stored in the loaded sample. In addition, it has been shown that the closer the specimen is to thermal equilibrium, the higher the heat loss [26]. A study investigating the heat concentration of a notched specimen showed a correlation between strain concentration and increased temperature at the vicinity of the crack tip [26]. These findings suggest that once a rubber sample is compromised by a crack, it will act as a local area of increased heat build-up. Therefore, it can be assumed that the higher the number of local cracks, the greater the heat build-up in that region. This assumption can be correlated with the damage to the specimens during CC wear. Thus, if the damage to the specimen increases beyond the number of impact cycles applied, the number of local cracks should increase simultaneously, which, in turn, leads to an increase in the rate of heat build-up in the local region. These heating phases are illustrated in Fig. 1 and described above.

Also, for CC wear, it has been proved that it depends on the mechanical load [8, 12, 27]. Therefore, a similar correlation between CC wear and heat evolution in the material can be assumed where, for example, in [12] for SBR, the temperature increased with increasing load. This trend has also been demonstrated for typical rubber formulation applied for tire tread [28, 29].

From an experimental point of view, only a very limited number of scientific studies are available on temperature measurements during CC wear. For example, in [8, 12, 27], a basic investigation of thermal evolution during CC analysis was performed, but the temperature measurement methodology was based on a simple IR temperature sensor that provided low-resolution data from one specific point on the surface of the analysed sample. Therefore, an advanced temperature measurement methodology based on high-speed thermography was required to obtain reliable and accurate thermal evolution data.

Therefore, this study focuses on describing the temperature evolution in the rubber specimen during CC wear for selected loading conditions at constant ambient temperature. The main objective was to obtain a detailed description of the temperature field at the surface of the rubber specimen for each impact and to characterize

its evolution as a function of an increasing number of loading cycles. The most important answer sought in the research was whether the temperature emerging during the CC process has a direct effect on CC wear.

Experiment and materials

Within the framework of the study, emulsion styrene–butadiene rubber (E-SBR 1500) was chosen to represent synthetic rubbers for the analyses. The compound was filled with 50 phr of carbon black (CB) of the type N330 and cross-linked with a sulphur-based curing system. Details about the ingredients and the complete formulation are listed in Table 1.

The rubber compound was prepared by two-step mixing process using an internal mixer SYD-2L (Everplast, Taiwan) of 1.5 L capacity and with a fill factor of 0.7. The first step consisted of preparing the master batch with a rotor speed of 50 rpm and mixing chamber temperature of 100 °C. Under these conditions, the virgin polymer was mixed for 1 min. Afterwards, the CB was added and mixed with raw polymer for additional 5 min, closing to a drop temperature of 150 °C. To finish master batch mixing, a double-roll mill with rolls' temperature of 60 °C was used to sheet the batch out.

The second step consisted of pre-mixing the master batch for 1 min at a rotor speed of 30 rpm under the initial temperature of 70 °C. Subsequently, the complete curing system was added and mixed for additional 2 min, reaching the drop temperature of 105 °C, thus completing the final batch. It was then milled and sheeted using a two-roll mill at a rolling temperature of 60 °C and stored for 24 h.

Then, the curing properties were measured using a moving die rheometer, MDR 3000 Basic (MonTech, Germany), according to ASTM 6204 at the temperature of 160 °C.

Three types of specimens were produced using a heat press LaBEcon (Fontijne Presses, The Netherlands) at a temperature of $T_t = 160$ °C for the optimal curing time of $t_{90} + 1$ min per 1 mm of thickness. First, standard sheets ($150 \times 150 \times 2$ mm) for ISO 37 Type 2 specimen were produced for the determination of tensile properties. Next, 6-mm-thick plates were fabricated for hardness testing. Finally, disc specimen with a diameter of 55 mm and a thickness of 13 mm were moulded for CC analyses. The production of test specimens was followed by measuring the tensile properties and Shore-A hardness. The tensile test was performed according to ISO 37 using the universal testing machine (Testometric, UK) at the strain rate of 500 mm/min for the Type S2 standardized specimen. The tensile properties presented in this study are averages of 5 replicates. The determination of the Shore-A hardness was carried out according to ISO 7619–1. Resulting hardness values are averages of 5 data points.

Finally, the CC behaviour with simultaneous thermal analysis was investigated using the Instrumented Cut and Chip Analyser in combination with high-speed thermo-camera (ImageIR® 9400, Infratec, Germany). The scheme and the photograph of the complete setup are shown in Fig. 3.

The principle of CC analysis using ICCA equipment has already been described by the authors in earlier publications, e.g. [8, 12, 27]. In the scheme shown in Fig. 3,

Table 1 Rubber compound formulation

Production steps	Ingredient	Chemical denotation	Type	Producer	Amount (phr)
Master batch	Polymer	Emulsion styrene–butadiene rubber	E-SBR BUNA® SB 1500	Synthos, Germany	100
	Filler	Carbon black	CB N330	Cabot, Czechia	50
Final batch	Antiozonant	*N*-(1,3-Dimethylbutyl)-*N*′-phenyl-*p*-phenylenediamine	6PPD	Lanxess, Germany	1
	Activator	Zinc oxide	ZnO	Slov-Zink a.s., Slovakia	2
	Activator	Octadecanoic acid	Stearic acid	Setuza a.s., Czechia	1
	Accelerator	*N*-tert-butylbenzothiazole-2-sulphenamide	TBBS	Duslo a. s., Slovakia	2
	Cross-linking agent	Sulphur	S	Estman Chemical, USA	2

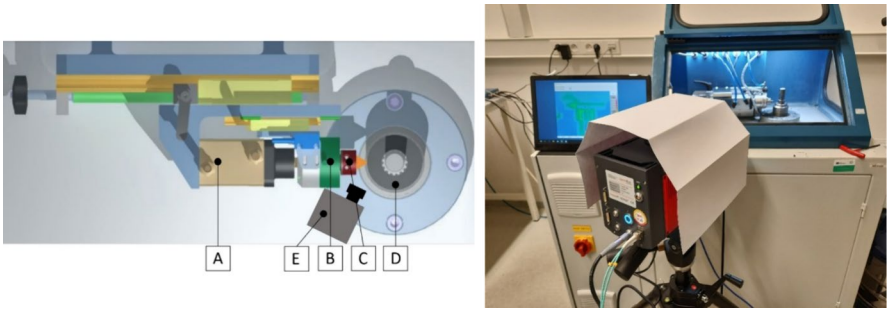

Fig. 3 Left: A schematic of the ICCA measuring principle, with: a pneumatic actuator (**A**); a two-axis load cell (**B**); a holder + impactor (**C**); a disc rubber test specimen (**D**) and a high-speed thermo-camera (**E**). Right: ICCA set-up with high-speed thermo-camera

the basic principle of CC analysis is based on applying a constant normal force, F_N, generated by a pneumatic actuator (*A*), to a rotating rubber sample with a disc geometry (*D*), while the triangular-shaped steel tool (*C*), whose geometry is shown in Fig. 4, simulates a bump that slides on the surface of the sample for a precisely defined sliding time, t_s. This cycle is repeated at a specific impact frequency, f_{imp} until the desired number of cycles, N_{imp} is reached. During the analysis, both the normal force and the tangential force are measured with a biaxial load cell (*B*). The analysis is performed at room temperature, and the heat generation during the CC analysis is measured in situ with a thermal camera (*E*).

Figure 5, left, shows the schematic representation of one impact cycle. During the rotation of the test sample at angular velocity, ω, the impacting tool is pushed into the test specimen at point *A* with a constant normal force, F_N. This constraint is released when the sample is rotated through an angle α, whereby the rotation time through this angle is equal to the sliding time, t_s. At point *B*, the contact between the tool and the specimen ends. This cycle is repeated at a defined impact frequency, f_{imp}. The diagram shown in Fig. 5, right, shows the progression of forces in this single impact cycle, with the normal force, F_N, being more or less constant throughout the sliding time, t_s, and the resulting tangential force, F_T, in response to the action of the normal force, having a lower slope to its maximum value, which is, however, higher than the value of the acting normal force. From the diagram in Fig. 5, right,

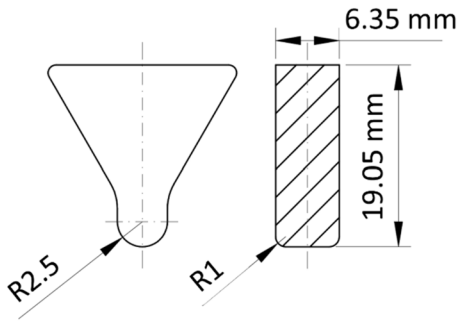

Fig. 4 The geometry of the impacting steel tool

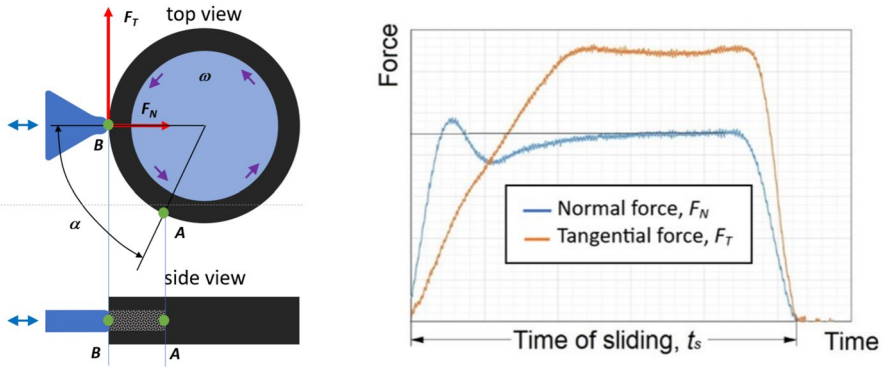

Fig. 5 Left: Principal scheme of the individual impact cycle; right: the shape of the measured normal, F_N, and tangential, F_T, forces

it can be clearly assumed that the character of the temperature evolution will follow the course of the forces during the sliding time, but the question is their exact shape and character.

As described in some previous publications, e.g. [11, 30, 31], the approach to determine the CC damage of rubber is based on the assignment of the resulting fluctuation of tangential force, F_T, in relation to the damaged sample surface.

If it is assumed that F_T increases proportionally with increasing roughness of the loaded surface, then the tangential force acts as a carrier of information about damage for every load cycle. To describe the damage not only in one cycle but also throughout the entire measurement, a numerical algorithm based on the tangential force over time is employed. A damage parameter P quantifies the CC damage via the number of cycles and represents a reciprocal equivalent to the CC resistance. More details about the calculation of the CC damage P parameter can be found, e.g. in [11].

Simultaneously, with the CC damage, the temperature was measured using a contactless method. Therefore, a high-speed thermo-camera was required to be calibrated by the emissivity factor obtained in the direct measurement of the sample temperature. This was performed using a highly precise contact temperature sensor Fluke 1524–256.

Finally, the resulting values of CC behaviour for SBR samples were evaluated along with the evolution of temperature on the surface of rubber sample throughout the CC analyses. The overall boundary conditions for the CC analyses examined in this study together with thermos-camera setting parameters are listed in Table 2.

Results and discussion

The mechanical properties of the compound determined from standard tensile testing as well as hardness Shore A test are summarized in Table 3. Five repetitions were used for hardness test as well as for tensile test.

Table 2 The CC testing conditions

Type of setup	Parameter	Value
ICCA	Normal force, F_N [N]	110, 150
	Rotation speed, ω [rpm]	203
	Sliding time, t_S [ms]	50
	Impact frequency, f_{imp} [Hz]	2
	Total number of cycles, N_{imp} [-]	(0), 1000, 2000, 3000
High-speed thermography	Sampling rate [Hz]	625
	Thermal range [°C]	30–150
	Thermal accuracy [°C]	1.2
	Thermal resolution [K]	0.03
	Image resolution [IR pixels]	1280 × 1024

Table 3 The Shore A and the tensile data

Hardness Shore A	Modulus 100 [MPa]	Modulus 300 [MPa]	Tensile strength [MPa]	Elongation at break [%]
64.4 ± 0.5	2.5 ± 0.1	10.9 ± 0.5	21.9 ± 1.6	501 ± 32

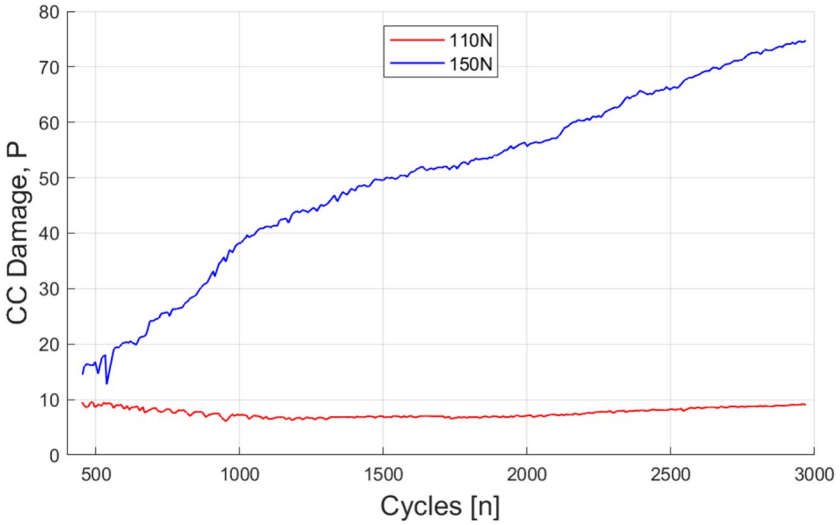

Fig. 6 CC damage P versus number of cycles

The CC behaviour of the analysed rubber compound with respect to the applied loading conditions, listed in Table 2, is plotted in Fig. 6. The analyses were performed for two different normal forces, and their influence is evident. For an applied force $F_N = 110$ N, the specimens showed a steady increase in CC

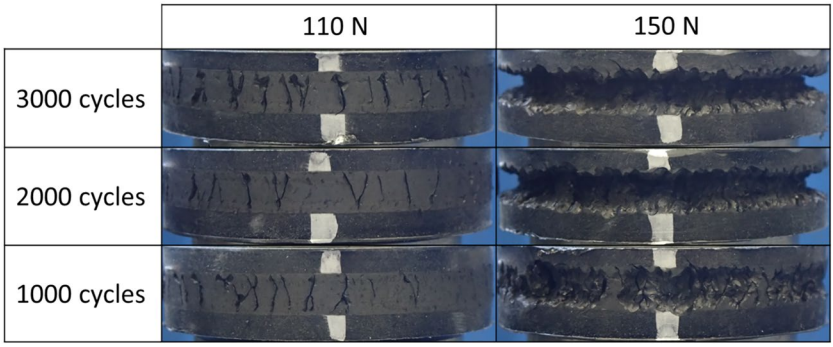

Fig. 7 Photographs of the ICCA specimen at chosen number of cycles

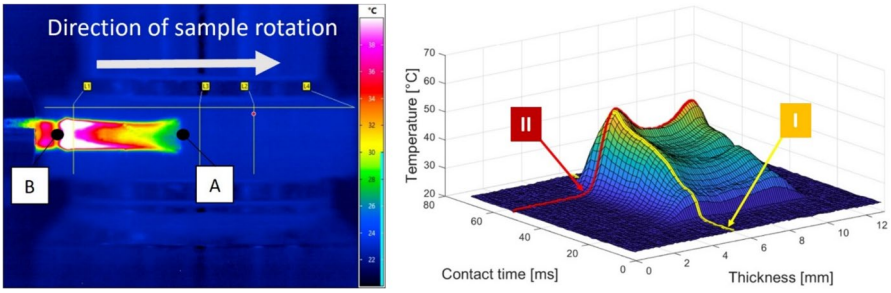

Fig. 8 Left: Thermographic record of the CC process and right: Evaluated temperature data over the process zone for an individual impact cycle

damage, *P*, during the first 400 cycles. In the analysis, the surface of samples was disturbed only by occasional cuts, as illustrated by the photographs of the sample surface damage for different numbers of impact cycles in Fig. 7. These cuts were shallow, and the force applied did not act sufficiently to widen and damage the surface in depth. Therefore, the values of the *P* parameter are more or less constant over the whole range of applied impact cycles (red curve in Fig. 6). On the other hand, the specimen subjected to an increased applied normal force, $F_N = 150$ N, showed a rapid increase in the CC damage, *P*, over the number of impact cycles (blue curve in Fig. 6). The applied normal force caused not only the initiation of the cuts, but also their propagation and subsequent break-off and chunk out of larger pieces of material. This trend corresponds to an increasing sample surface damage with an increasing number of impact cycles, as can be clearly seen from Fig. 7.

The obtained results of CC damage, *P,* are consistent with the previous findings [11, 30, 31], which also found that the CC wear of SBR rubber increases with increasing normal force. Figure 8, left, illustrates the thermographic record taken by the high-speed thermal imaging camera for the first impact cycle. The start of the impact cycle is labelled A in the thermogram, and it is the moment

when the steel tool first touches the sample surface. Furthermore, the record of the temperature evolution on the surface during the period of friction between the steel tool and the sample as it rotates through the angle α during the sliding time t_s is clearly visible. Point B then marks the end of the contact between the tool and the surface of the sample. The thermogram then clearly demonstrates the temperature development from point *A* to point *B* in such a way that the temperature increases in the direction from point A, where the steel tool impacts the rubber, to point *B*. The highest temperature is measured in the vicinity of this point, where the contact ends. In the analyses of the temperature evolution over the width of the contact trace, it can also be seen that the highest temperature occurs in the edge regions of the contact between the steel tool and the rubber surface. Then, towards the centre, the temperature decreases from both extreme positions. The 3D diagram in Fig. 8, (right), represents the temperature distribution in this area from point *A* to point *B* over the entire contact time. The absolute values confirm the above observations. To further describe the data in this study, the 3D diagram is divided into two sections, Plane I and Plane II. Plane I represents the dependence of temperature on the contact time, whereas Plane II represents the dependence of temperature on sample thickness.

As shown in Fig. 8 (right), this is the temperature distribution in the ideal case, when the surface of the sample is not stressed with any previous impact cycle. However, in real tire operation in heavy terrain, random impacts occur anywhere on the tread surface, where sequential impacts may partially or completely overlap. Therefore, the applied test method takes this possible overlapping of impacts into account and simulates it in a defined way, which is schematically shown in Fig. 9. This diagram illustrates a realistic situation where the first impact is on a completely fresh surface running for a sliding time, t_s, from the start of contact at point A_1 to point B_1. However, the second impact takes place with a delay defined as impact delay, t_{id}, which defines the time interval between the original position of point A_1 and the new position of point A_2. The identical delay also applies to the time interval between points B_1 and B_2. The completely constant time delay, t_d, then applies to all subsequent impacts.

Figure 10 then shows the thermal camera footage that captures the overlay of the first and second impacts. It can be seen that the temperature in the overlap region from A_2 to B_2 is higher than in the first impact region shown in Fig. 8, left. However, it is important to note that each subsequent impact occurs as the sample rotates, with the first impact region cooling from A_1 to A_2 as sample rotates.

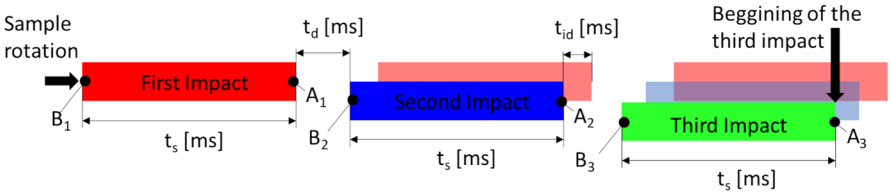

Fig. 9 Timing scheme of sequential impacts

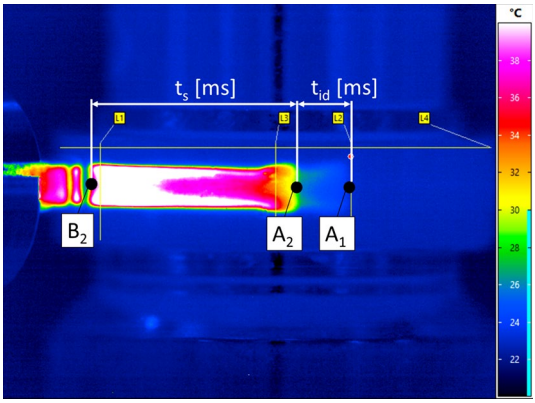

Fig. 10 Thermogram recording the overlap of impacts

From the series of Figs. 8, 9 and 10, it can be seen that only the first impact is completely unaffected by a CC process, but each subsequent impact afterwards is influenced by an overlap from one of the previous impacts. This has a major effect on the CC wear as well as on the resulting rubber temperature during the CC process. The diagrams in Fig. 11 show the temperature evolution in Plane I for three different numbers of impact cycles, namely for the very first cycle, for 2000 and 3000 impact cycles. The figure on the left shows the values of temperature evolution for the normal force $F_N = 110$ N, and on the right, for $F_N = 150$ N.

The temperature evolution for $F_N = 110$ N shows a continuous temperature increase from the initial contact between the tool and the surface of the sample until its end. However, in the case of a higher number of impact cycles, the temperature increase occurs during the penetration of the tool into the sample, after reaching a constant normal force. Then, the temperature is more or less constant throughout the sliding period until the tool leaves contact. The highest temperature range is between the first and the 2000th cycle, which is about 50 °C, and the temperature trends as absolute values between 2000 and 3000 cycles are almost identical. It can, therefore, be assumed that after 2000 cycles, the temperature of rubber was already completely stabilized and reached its equilibrium.

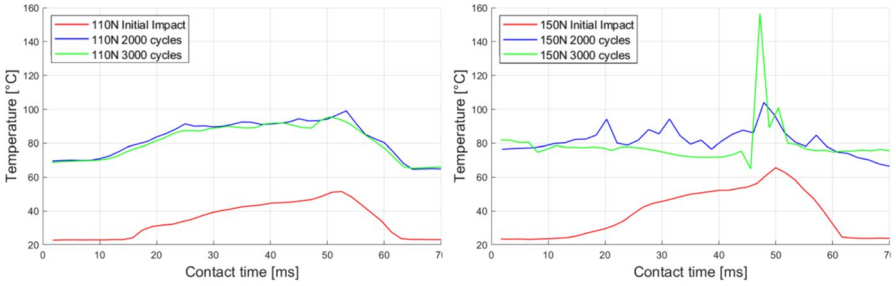

Fig. 11 Temperature data along the path of a hit for $F_N = 110$ N (left) and $F_N = 150$ N (right) at chosen number of cycles

In the case of temperature development in the rubber loaded with a higher normal force, $F_N = 150$ N, the temperature vs. contact time curve (see Fig. 11) for the first impact cycle is the same as in the case of the lower force, but here one reaches significantly higher absolute values by about 20 °C. For the two higher impact cycles, 2000 and 3000, the curve is identical and is more or less constant over the sliding time as well as out of this region. This constant temperature over the entire circumference of the sample can be explained by the fact that the specimen was already severely damaged by CC wear at a certain number of cycles and, therefore, the measured temperature corresponds to the temperature value in the depth of the sample, which was constant due to the temperature concentration in the material volume and corresponds to the value of a saturated temperature. The high isolated peak in the curve for 3000 cycles corresponds to the temperature development when the tool impacts a pothole in the wear depth of the sample, with enormous deformation and, therefore, also high-temperature development. These peaks are characteristic for the advanced state of CC wear. It can, therefore, be said that the specimen is more damaged by CC wear, the higher temperature peaks are manifested, which can be traced from all the curves shown in Fig. 11. The curves for the first impact cycles are more or less smooth. In the case of the normal force $F_N = 110$ N, minimal peaks are visible in both curves and of the same nature as the absolute magnitudes of the temperature for both 2000 and 3000 cycles. This is quite correlated with the CC damage photographs for these cycles shown in Fig. 7, where the damage is independent of the number of impact cycles. However, if we compare the curves for a normal force of $F_N = 150$ N, it is quite clear that the comparison between the smooth curve for the first cycle and the curve for 2000 cycles already shows a significant number of temperature peaks. For 3000 cycles, only one temperature peak is visible, but its absolute value is significantly higher than of the peaks in the case of 2000 cycles. When compared with the photographs of CC damage shown in Fig. 7, it is evident that CC damage increases with increasing cycles, and hence, the absolute value of the temperature peaks must also increase.

Figure 12 shows the temperature profile within the Plane II (see Fig. 8, right) for both applied normal forces and for the three different numbers of impact cycles specified in Table 2. From the temperature profiles in the first impact cycle for both normal forces, it can be seen that the temperature is highest in the peripheral parts

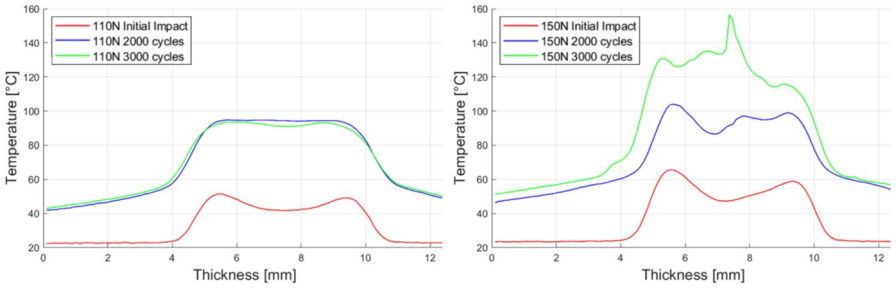

Fig. 12 Temperature data from cross-section at the end of a hit for $F_N = 110$ N (left) and $F_N = 150$ N (right) at chosen number of cycles

of the profile, where the edges of the tool are in contact with the rubber. The temperature slightly decreases towards the centre. However, this phenomenon decreases as the number of cycles increases until a constant temperature value is reached over the entire profile. The increased temperature in the edge areas is obviously due to the increased stress concentration in this area, the deformations there being caused by the rounded corner of the tool, while the rubber in the centre is influenced by the cylindrical surface, which causes lower stresses than in the edge areas. The disappearance of this phenomenon as the number of cycles increases can be attributed to the fatigue effect of the rubber in the case of a lower normal force $F_N = 110$ N, when the result of the fatigue is a lower stress and its uniform distribution over the deformation profile. In the case of the higher normal force $F_N = 150$ N, however, the result is different. The rubber, which is subjected to a high load, is subject to CC wear very quickly, so that the breakouts in the centre of the profile are subject to strong deformation and strong heat generation.

It can also be seen that as the number of cycles increases, the extreme CC wear increases and the temperature in the centre begins to exceed the values of the boundary temperature, as can be seen from the curve describing the temperature evolution profile at 3000 cycles (see Fig. 12, right). It can also be seen from the graphs that the temperature profiles for the lower normal force are identical at 2000 and 3000 impact cycles, while the temperature profile for the higher normal force increases as the number of cycles increases. Finally, it can be seen that the absolute value of the temperature also increases with increasing normal force.

Figure 13 shows photographs of the section through the samples for each normal force and the numbers of analysed impacting cycles. The photographs show the worn profile in Plane II (see Fig. 8, right). It is evident that for the applied normal force, $F_N = 110$ N, the depth of the profile is almost constant for all analysed impact cycles. However, for the increased normal force, the absolute depth of the profile is higher compared to lower normal force; moreover, the profile depth increases with

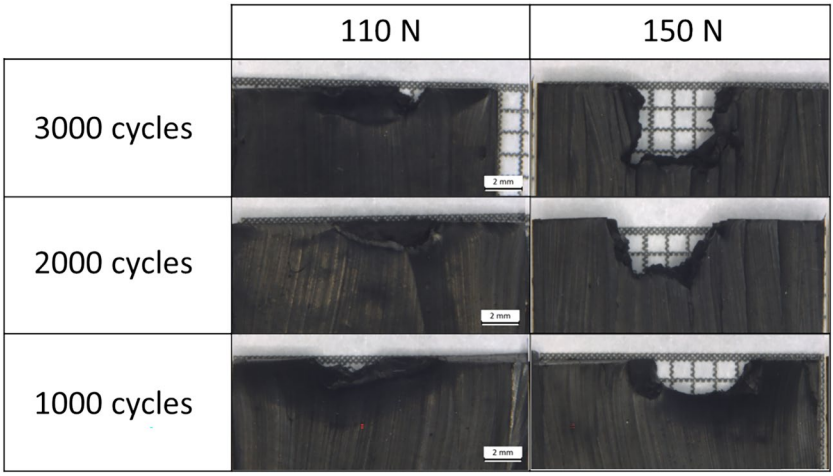

Fig. 13 Photographs of the cross-sectioned ICCA specimen at chosen number of cycles

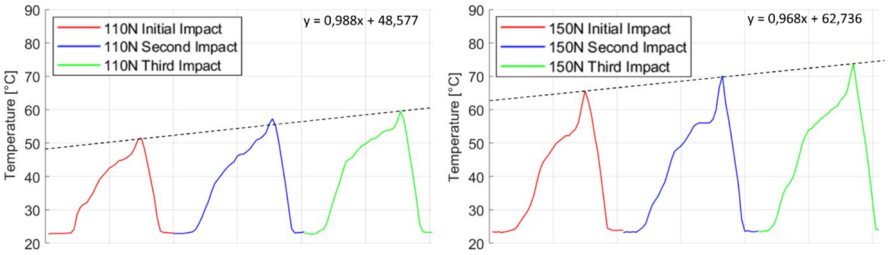

Fig. 14 Temperature data of three sequential hits along the path of a hit for $F_N = 110$ N (left) and $F_N = 150$ N (right)

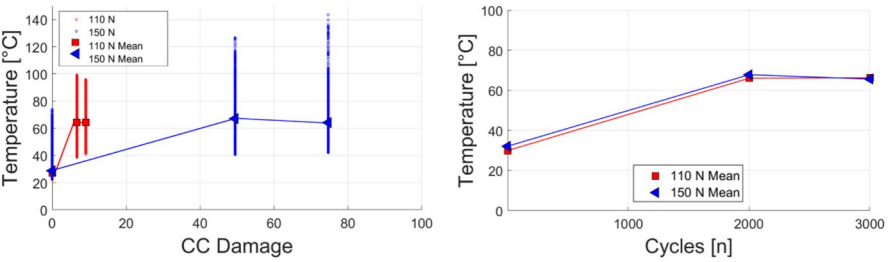

Fig. 15 Temperature over CC damage, P (left) and temperature over number of cycles (right)

increasing number of applied impact cycles. The shape of the profile, especially for the samples subjected to higher normal force at 2000 and 3000 cycles, also shows significant wear in the corner regions, which can be attributed to the stress concentration and increased temperature in this area.

Figure 14 shows the temperature evolution for the first three impact cycles for both applied normal forces.

For both normal forces, the individual impact data follow the same trend with increasing temperature over the contact time, peaking at the end of the contact. At the same time, the temperature peaks gradually increase with the number of impacts. This increase provides information on the ability of the material to absorb and store the thermal energy generated by the friction between the impact tool and the surface of the rubber specimen. When comparing the temperature data, a clear difference in absolute values can be observed, with peaks for higher normal force showing approximately 14 °C higher temperature. Figure 14 further shows that the increase in the maximum temperature values for the first three impacts is linear and independent of the applied normal force. This load independence is evident from the almost identical exponents of the slopes of the two curves (see Fig. 14), where the difference is negligible. Thus, it can be concluded that at the beginning of the CC wear process, the initial temperature value depends on the value of the selected normal force, but the temperature rise during the first three cycles does not.

The diagram in Fig. 15, left, shows the temperature dependence on CC damage, P for both applied normal forces. The plotted values, indicated by solid red squares and blue triangles symbols, are the mean values of the temperature of a given impact

for the current number of cycles. The empty circle symbols then represent all measured values that correspond to all values of the 3D temperature profile shown in Fig. 8, right. Figure 15, right, shows the dependence of the average temperature values on the number of impact cycles. From the diagrams, it can be seen that the wear temperature of the CC wear increases with increasing number of cycles up to the thermal equilibrium value that occurs at a certain number of impact cycles. For the analysed SBR, this thermal equilibrium occurs at approximately 2000 impact cycles.

This trend is consistent with the previous findings regarding temperature rise in rubber materials and specifically thermal equilibrium [21, 22, 25]. A very important observation is that the temperature evolution over increasing number of impact cycles is independent of the applied load, but at the same temperature and number of cycles, very different CC wear occurs for different loads. This can be observed in the final CC damage values of $P = 10$ with temperature just above 65 °C for $F_N = 110$ N, while for $F_N = 150$ N, the final CC damage $P = 75$, but the measured temperature is comparably close to 65 °C.

From this, a very important finding can be concluded, namely that the development of temperature during CC wear is dependent on the applied material, i.e. it is a material property and is completely independent of the applied load for a given number of impact cycles. Moreover, for different CC wear, the same temperature development occurs within the material for a given number of impact cycles.

Conclusion

The present work deals with the effects of self-heating on rubber abrasion during cut and chip (CC) wear. The main objective was to obtain information on the extent to which CC wear is dependent on heat generation in the rubber.

In this study, an experimental investigation of heat generation during the CC wear process of SBR-based rubber compounds was conducted. Moreover, the temperature development within a single impact cycle during the CC wear is examined in detail for the first time, and the evolution of temperature is tracked as a function of the increasing number of impact cycles and thus the progression of CC wear. This methodology was based for the first time on a combination of the use of laboratory instrumented equipment for CC wear analysis and high-speed thermography. The combination of these two methods ensured high accuracy in the analysis of temperature evolution during CC wear under reproducible laboratory conditions.

In terms of mechanical behaviour, it was confirmed that the higher the applied load, the higher the CC wear of the SBR rubber, which is consistent with the previous findings on the resistance of synthetic rubber to CC wear. However, from a thermal point of view, it is surprising to find that the temperature development during CC wear of SBR rubber is completely independent of the applied load. It was also found that at the beginning of the CC wear process, the initial temperature value depends on the applied load, but the temperature rise during the first CC wear phase does not. Last but not least, it has been demonstrated unanimously that during CC wear, the temperature rises up to a certain level, and then, the temperature does not rise any further, but the generated heat leaves to the surroundings.

The load dependence of CC abrasion of different rubbers has already been fully demonstrated, but the load independence of heat generation for SBR rubber analysed in this study needs to be verified in future studies aimed at analysing the temperature evolution during CC abrasion of different materials.

Such data could then be used for advanced numerical simulations of different tire wear processes or, for example, off-segment tires for CC of conveyor belt tread wear, as well as for intelligent optimization of rubber compounds to improve the wear resistance of these different applications.

Acknowledgements This work was supported by the Ministry of Education, Youth and Sports of the Czech Republic—DKRVO (RP_CPS_2024_28_006). The authors are also grateful for the funding of the grant received from The Internal Grant Agency (IGA) of TBU in Zlin—(IGA/CPS/2024/001).

Author contributions N.R. contributed to manuscript writing, data evaluation and figures preparation. R.S. contributed to manuscript writing and manuscript review. M.S. helped in data colection. J.M. helped in data colection and data evaluation.

Funding Open access publishing supported by the National Technical Library in Prague.

Data availability No datasets were generated or analysed during the current study.

Declarations

Conflict of interest The authors declare no competing interests.

References

1. Klüppel M (2014) Wear and abrasion of tires. In: Kobayashi S, Müllen K (eds) Encyclopedia of polymeric nanomaterials. Springer, Berlin, Heidelberg. https://doi.org/10.1007/978-3-642-36199-9_312-1
2. Heinrich G, Klüppel M (2022) Basic mechanisms and predictive testing of tire-road abrasion. In: Heinrich G, Kipscholl R, Stoček R (eds) Degradation of elastomers in practice, experiments and modelling. Advances in polymer science, vol 289. Springer, Cham. https://doi.org/10.1007/12_2022_113
3. Schallamach A (1968) Recent advances in knowledge of rubber friction and tire wear. Rubber Chem Technol 41:209–244. https://doi.org/10.5254/1.3539171
4. Grosch KA (1992) Abrasion of rubber and its relation to tire wear. Rubber Chem Technol 65(1):78–106. https://doi.org/10.5254/1.3538609
5. Gent AN, Nah C (1996) Abrasion of rubber by a blade abrader: effect of blade sharpness and test temperature for selected compounds. Rubber Chem Technol 69(5):819–833. https://doi.org/10.5254/1.3538405

6. Pacejka HB, Sharp RS (1991) Shear force development by pneumatic tyres in steady state conditions: a review of modelling aspects. Veh Syst Dyn 20(3–4):121–175. https://doi.org/10.1080/00423119108968983
7. Pacejka HB (2005) Tyre and vehicle dynamics, 2nd edn. Elsevier
8. Kipscholl R, Stocek R (2022) Degradation of tires during intended usage. Degradation of elastomers in practice, experiments and modeling. Springer International Publishing, Cham, pp 185–207. https://doi.org/10.1007/12_2022_132
9. Beatty J, Miksch B (1982) A laboratory cutting and chipping tester for evaluating off-the-road and heavy-duty tire treads. Rubber Chem Technol 55(5):1531–1546. https://doi.org/10.5254/1.3535947
10. Nah C, Jo BW, Kaang S (1998) Cut and chip resistance of NR–BR blend compounds. J Appl Polym Sci 68(9):1537–1541. https://doi.org/10.1002/(SICI)1097-4628(19980531)68:9%3c1537::AID-APP17%3e3.0.CO;2-W
11. Stocek R, Mars WV, Kipscholl R, Robertson CG (2019) Characterisation of cut and chip behaviour for NR, SBR and BR compounds with an instrumented laboratory device. Plast Rubber Compos 48(1):14–23. https://doi.org/10.1080/14658011.2018.1468161
12. Stocek R, Heinrich G, Kipscholl R, Kratina O (2021) Cut & chip wear of rubbers in a range from low up to high severity conditions. Appl Surf Sci Adv 6:100152. https://doi.org/10.1016/j.apsadv.2021.100152
13. Stocek R, Heinrich G, Schulze A, Wunde M, Kluppel M, Vatterott C, Tschimmel J, Laycayo-Pineda J, Kipscholl R (2020) Chip & cut wear of truck tire treads: comparison between laboratory and real tire testing. KGK-Kautschuk Gummi Kunststoffe 73(6):51–55
14. Hirata Y, Kondo H, Ozawa Y (2014) Natural rubber (NR) for the tyre industry. Chemistry, manufacture and applications of natural rubber. Woodhead Publishing, pp 325–352. https://doi.org/10.1533/9780857096913.2.325
15. Gent AN, Hindi M (1988) Heat build-up and blowout of rubber blocks. Rubber Chem Technol 61(5):892–905. https://doi.org/10.5254/1.3536225
16. Medalia AI (1991) Heat generation in elastomer compounds: causes and effects. Rubber Chem Technol 64(3):481–492. https://doi.org/10.5254/1.3538565
17. Gschwandl M, Kerschbaumer RC, Schrittesser B, Fuchs PF, Stieger S, Meinhart L (2019) Thermal conductivity measurement of industrial rubber compounds using laser flash analysis: applicability, comparison and evaluation. In: AIP conference proceedings. AIP Publishing. https://doi.org/10.1063/1.5088299
18. Lion A (1997) On the large deformation behaviour of reinforced rubber at different temperatures. J Mech Phys Solids 45(11–12):1805–1834. https://doi.org/10.1016/S0022-5096(97)00028-8
19. Gent AN (2012) Engineering with rubber: how to design rubber components. Carl Hanser Verlag GmbH Co KG
20. Ayoub G, Nait-Abdelaziz M, Zairi F (2012) Fatigue life prediction of rubber-like materials under multiaxial loading using a continuum damage mechanics approach: effects of two-blocks loading and R ratio. Mech Mater 52:87–102. https://doi.org/10.1016/j.mechmat.2012.03.012
21. Kratina O, Stocek R, Voldanova J (2022) How the rubber compounds of different tire's components heat up?. In: Constitutive models for rubber XII: proceedings of the 12th european conference on constitutive models for rubber (ECCMR 2022), September 7–9, 2022, Milano, Italy. CRC Press, p 199. https://doi.org/10.1201/9781003310266-34
22. Rodas CO, Zairi F, Nait-Abdelaziz M (2014) A finite strain thermo-viscoelastic constitutive model to describe the self-heating in elastomeric materials during low-cycle fatigue. J Mech Phys Solids 64:396–410. https://doi.org/10.1016/j.jmps.2013.10.010
23. Larin AA, Vyazovichenko YA, Barkanov E, Itskov M (2018) Experimental investigation of viscoelastic characteristics of rubber-cord composites considering the process of their self-heating. Strength Mater 50:841–851. https://doi.org/10.1007/s11223-019-00030-7
24. Luo W, Huang Y, Yin B, Jiang X, Hu X (2020) Fatigue life assessment of filled rubber by hysteresis induced self-heating temperature. Polymers 12(4):846. https://doi.org/10.3390/polym12040846
25. Dedova S, Schneider K, Heinrich G (2017) Influence of dissipative specimen heating on the tearing energy of elastomers estimated by global and local characterization methods. Constitutive models for rubber X. CRC Press, Boca Raton, pp 219–224
26. Dedova S, Schneider K, Stommel M, Heinrich G (2021) Dissipative heating, fatigue and fracture behaviour of rubber under multiaxial loading. Fatigue crack growth in rubber materials: experiments and modelling. Springer, Cham, pp 421–443. https://doi.org/10.1007/12_2020_75

27. Poschl M, Stocek R, Zadrapa P (2022) The effect of apparent cross-link density on cut and chip wear in natural rubber. Degradation of elastomers in practice, experiments and modeling. Springer International Publishing, Cham, pp 273–291. https://doi.org/10.1007/12_2022_129
28. Chang X, Huang H, Jiao R, Liu J (2020) Experimental investigation on the characteristics of tire wear particles under different non-vehicle operating parameters. Tribol Int 150:106354. https://doi.org/10.1016/j.triboint.2020.106354
29. Li Y, Zuo S, Lei L, Yang X, Wu X (2012) Analysis of impact factors of tire wear. J Vib Control 18(6):833–840. https://doi.org/10.1177/1077546311411756
30. Stoček R, Ghosh P, Machů A, Chanda J, Mukhopadhyay R (2020) Fatigue crack growth vs. chip and cut wear of NR and NR/SBR blend-based rubber compounds. In: Heinrich G, Kipscholl R, Stoček R (eds) Fatigue crack growth in rubber materials. Advances in polymer science, vol 286. Springer, Cham. https://doi.org/10.1007/12_2020_67
31. Pöschl M, Stoček R, Zádrapa P (2022) The effect of apparent cross-link density on cut and chip wear in natural rubber. In: Heinrich G, Kipscholl R, Stoček R (eds) Degradation of elastomers in practice, experiments and modelling. Advances in polymer science, vol 289. Springer, Cham. https://doi.org/10.1007/12_2022_129